Original article

Evaluation of apoptotic effects of mPEG-b-PLGA coated iron oxide nanoparticles as a eupatorin carrier on DU-145 and LNCaP human prostate cancer cell lines

Marziyeh Shalchi Tousi [a], Houri Sepehri [a, *], Sepideh Khoee [b], Mahdi Moridi Farimani [c], Ladan Delphi [a], Fariba Mansourizadeh [a]

[a] Department of Animal Biology, School of Biology, College of Science, University of Tehran, Tehran, Iran
[b] Polymer Chemistry Department, School of Science, University of Tehran, Tehran, Iran
[c] Department of Phytochemistry, Medicinal Plants and Drugs Research Institute, Shahid Beheshti University, Tehran, Iran

ARTICLE INFO

ABSTRACT

Many studies have so far confirmed the efficiency of phytochemicals in the treatment of prostate cancer. Eupatorin, a flavonoid with a wide range of phytomedical activities, suppresses proliferation of and induces apoptosis of multiple cancer cell lines. However, low solubility, poor bioavailability, and rapid degradation limit its efficacy. The aim of our study was to evaluate whether the use of mPEG-b-poly (lactic-co-glycolic) acid (PLGA) coated iron oxide nanoparticles as a carrier could enhance the therapeutic efficacy of eupatorin in DU-145 and LNCaP human prostate cancer cell lines. Nanoparticles were prepared by the co-precipitation method and were fully characterized for morphology, surface charge, particle size, drug loading, encapsulation efficiency and in vitro drug-release profile. The inhibitory effect of nanoparticles on cell viability was evaluated by MTT test. Apoptosis was then determined by Hoechest staining, cell cycle analysis, NO production, annexin/propidium iodide (PI) assay, and Western blotting. The results indicated that eupatorin was successfully entrapped in Fe_3O_4@mPEG-b-PLGA nanoparticles with an efficacy of $(90.99 \pm 2.1)\%$. The nanoparticle's size was around (58.5 ± 4) nm with a negative surface charge $[(-34.16 \pm 1.3)$ mV]. In vitro release investigation showed a 30% initial burst release of eupatorin in 24 h, followed by sustained release over 200 h. The MTT assay indicated that eupatorin-loaded Fe_3O_4@mPEG-b-PLGA nanoparticles exhibited a significant decrease in the growth rate of DU-145 and LNCaP cells and their IC50 concentrations were 100 μM and 75 μM, respectively. Next, apoptosis was confirmed by nuclear condensation, enhancement of cell population in the sub-G1 phase and increased NO level. Annexin/PI analysis demonstrated that eupatorin-loaded Fe_3O_4@mPEG-b-PLGA nanoparticles could increase apoptosis and decrease necrosis frequency. Finally, Western blotting analysis confirmed these results and showed that Bax/Bcl-2 ratio and the cleaved caspase-3 level were up-regulated by the designing nanoparticles. Encapsulation of eupatorin in Fe_3O_4@mPEG-b-PLGA nanoparticles increased its anticancer effects in prostate cancer cell lines as compared to free eupatorin. Based on these results, this formulation can provide a sustained eupatorin-delivery system for cancer treatment with the drug remaining active at a significantly lower dose, making it a suitable candidate for pharmacological uses.
© 2020 Xi'an Jiaotong University. Production and hosting by Elsevier B.V. This is an open access article under the CC BY-NC-ND license (http://creativecommons.org/licenses/by-nc-nd/4.0/).

1. Introduction

Prostate cancer is the second most common cancer among men and the fourth most common cancer all over the world. Almost 1.3 million new cases of prostate cancer and 359,000 associated deaths worldwide were estimated in 2018 [1]. During the past few decades, prostate cancer incidence was reported to be much lower among Asian people [2]. One basic reason is that their normal meal contains flavonoids-rich components (from vegetables, fruits, and other natural products) [3].

Flavonoids are widely identified as a class of natural products with cancer protective properties through multifactorial pathways

[4]. Eupatorin, a natural methoxyflavone isolated from several plants, has been shown to exhibit anti-proliferative [5], anti-angiogenesis [6], anti-inflammatory [7] and cytotoxic properties [8] in cell culture studies in vitro and in vivo.

Although the use of natural products for the prevention and treatment of prostate cancer has shown promising results in pre-clinical testing, their use on humans has had several challenges [9]. In general, flavonoids have an inappropriate pharmacokinetic profile (i.e., absorption, distribution, metabolism, excretion, and toxicity), determined by inefficient systemic delivery, very short half-life in plasma, low aqueous solubility, limited bioavailability, poor oral absorption, negligible cellular uptake and extensive first pass metabolism [10–12]. Also, the poor chemical stability of fla-vonoids has been shown to restrict their usefulness and several factors, such as oxygen exposure, temperature, light, ultraviolet radiation and pH, were shown to reduce their stability and result in their subsequent degradation [13]. These properties lead to using higher doses of such drugs resulting in systemic toxicity [14].

Despite the challenges in the use of natural products, the liter-ature suggests that nanotechnology provides a novel system for the delivery of herbal medicines and active constituents [15]. Nano-herbal drug delivery system has many advantages including improving the solubility, stability and bioavailability of the drug, promoting its sustained release to increase the pharmacological effects, reducing the required dose, toxicity and side effects, and protecting the drug against possible physical and chemical degra-dation [16,17].

A variety of novel nanoparticles have been reported to deliver cancer therapeutics [18]. Super paramagnetic iron oxide nano-particles (SPIONs) are the only magnetic nanoparticles approved for clinical application by the US Food and Drug Administration (FDA) [19], which have been investigated as carriers for targeted drug delivery [20]. They have low toxicity, remain in circulation for a long time, and are usually biodegradable. Nevertheless, the up-take of SPIONs by the target cells is inefficient due to the negative charge on both the plasma membrane and the SPION surface. Therefore, a complex coating fabricated from transduction agents is often applied to raise the nanoparticles' labeling efficiency [21].

Amphiphilic block copolymers are one of the most successfully used biodegradable polymers to enhance the uptake of SPIONs by cancer cells. One of the blocks is hydrophilic, poly (ethylene glycol) (mPEG), and the other one is hydrophobic, poly (lactic-co-glycolic) acid (PLGA). Recently, numerous publications have reported PLGA-based nanotechnologies in drug delivery because they are highly biocompatible [22] and can enhance molar relaxivity of the Fe and cellular internalization [23]. These nanosystems allow the assess-ment of drug biodistribution, optimization of strategies and real-time monitoring of therapeutic responses [24].

The main purpose of our study was to design an appropriate nano-based drug delivery system to promote eupatorin efficiency. We compared the inhibitory effects of free eupatorin and eupa-torin-loaded Fe_3O_4@mPEG-b-PLGA nanoparticles on cell viability in DU-145 and LNCaP human prostate cancer cell lines. In so doing, SPIONs nanoparticles stabilized with oleic acid were synthesized and subsequently coated by mPEG-b-PLGA as a eupatorin carrier. We completely characterized the nanoparticles and cytotoxicity was determined by different apoptotic detection tests.

2. Materials and methods

2.1. Reagent and antibody

Poly(ethylene glycol) methyl ether-*block*-poly(lactide-co-glyco-lide) or mPEG-b-PLGA (PEG average Mn 5,000, PLGA Mn 7000), oleic acid, 3-(4,5-dimethylthiazol-2-yl)-2,5-diphenyltetrazolium bromide) (MTT), Hoechst 33342, Dil 42364, sulfanilamide, N-1-naphthyl ethylenediamine dihydrochloride (NED) and RNase A were bought from Sigma Aldrich Co. (UK). The antibodies directed against Bax, Bcl-2, Caspase-3, and β-actin were obtained from Cell Signaling Technology (Danvers, Massachusetts, USA). RPMI 1640 media, fetal bovine serum (FBS), penicillin–streptomycin and trypsin/EDTA were purchased from Gibco Co. (Grand Island, USA). Electrochemiluminescence (ECL) reagents and polyvinylidene fluoride (PVDF) membranes were purchased from Amersham Bioscience (Arlington Heights, USA). Annexin V-Fluos staining kit was purchased from Roche Life Science (Penzberg, Germany).

Nuclear magnetic resonance (NMR) spectra were recorded on a Bruker DRX-500 Avance spectrometer operated at 500.13 MHz for ^1H and 125.77 MHz for ^{13}C, using a 5 mm QNP probe. $CDCl_3$ for NMR was purchased from Armar Chemicals. Chemical shifts were expressed in ppm, and the residual $CDCl_3$ signal (δ_H 7.27/δ_C 77.0) as the reference [25].

2.2. Plant material

The aerial parts of *Salvia mirzayanii* were collected in March 2011 on Genu Mountain in Bandar Abass area of Southern Iran. The plant material was identified by Mr. Soltanipoor, Agricultural and Natural Resources Center (ANRC) of Hormozgan, Bandar Abbass, Iran, and a voucher specimen (5322) was deposited in the herbar-ium of ANRC.

2.3. Extraction and isolation of eupatorin

The dried plant material (4.5 kg) was ground and extracted by maceration with *n*-hexane (5 × 25 L), acetone (5 × 25 L), and MeOH (5 × 25 L). Evaporation of the acetone extract afforded 125 g of a dark gummy residue. The extract was separated on a silica gel column (230–400 mesh, 127.0 cm × 5.0 cm, 750 g) with a gradient of *n*-hexane-EtOAc (100/0 to 0/100) as eluent, followed by increased concentration of MeOH (up to 25%) in EtOAc. After screening by TLC (thin layer chromatography), fractions with similar compositions were pooled to yield 30 combined fractions. Fraction 16 [eluted with hexane-EtOAc (55:45, *V/V*)] contained a crude solid, which was triturated with Me_2CO to yield eupatorin (250 mg).

2.4. Cell culture condition

Human prostate cancer cell lines (DU-145 and LNCaP) and hu-man umbilical vein endothelial cell line (HUVEC) were obtained from NCBI (National Cell Bank of I.R. Iran) and grown in RPMI 1640 medium supplemented with 10% heat inactivated FBS. All cells were cultured at 37 °C in a humidified incubator with 5% CO_2.

2.5. Synthesis of nanoparticles

Magnetic nanoparticles (Fe_3O_4) were synthesized [26] and oleic acid surface modification was performed based on the previously described method [27].

Synthesis of eupatorin-loaded Fe_3O_4@mPEG-b-PLGA nano-particles was based on the nano-precipitation method according to previously published data [28]. Briefly, 30 mg of Fe_3O_4 nanoparticle modified with oleic acid was dispersed in 2 mL of acetone and sonicated for 10 min (5 s on/3 s off) using the Bandelin probe sonicator to obtain a homogeneous suspension. On the other hand, 10 mg of eupatorin was dissolved in 2 mL of acetone and mixed well for 2 min, followed by the addition of 70 mg of mPEG-b-PLGA. The compound was then completely dissolved and added to iron oxide nanoparticle suspension. The mixture was vortexed for 10 min

without interruption and finally drop wised in 40 mL of deionized water on a magnetic stirrer. Then, acetone was evaporated in a rotary evaporator and the remaining contents were freeze-dried to remove the water without destroying the nanoparticle structures.

Additionally, mPEG-b-PLGA coated iron oxide nanoparticles without eupatorin were prepared in the same way as a control sample.

2.6. Characterization of nanoparticles

2.6.1. Dynamic light scattering (DLS)

The mean diameter, size distribution and surface charge (zeta potential) of the nanoparticles in the aqueous dispersion were measured by the same instrument, Zetasizer Nano ZS (Malvern Instruments) at 25 °C. Briefly, 1 mg of the nanoparticles was dispersed in 2 mL of deionized water and sonicated for 10 min. The hydrodynamic size average of the nanoparticles was determined by DLS. Afterward, samples were placed in an electrophoretic cell and zeta potential was measured.

2.6.2. Thermal gravimetric analysis (TGA)

The presence and proportion of organic compounds onto the surfaces of magnetite mPEG-b-PLGA nanoparticles were investigated by TGA Q50 V6.3 Build 189. The temperature of the sample gently increased from room temperature to 600 °C at the rate of 10 °C/min under nitrogen atmosphere. Moreover, the presence of mPEG-b-PLGA on magnetite nanoparticles surface was confirmed by TGA as mentioned above.

2.6.3. Transmission electron microscopy

The morphological investigation of nanoparticles and the selected area electron diffraction (SAED) pattern was done using a Zeiss LEO 906 transmission electron microscopy (TEM). The nanoparticle was dispersed in distilled water and sonicated for 10 min. A drop of nanoparticle suspension was placed on the TEM grid (carbon coated 200 mesh cupper grid, TED PELLA INC., USA). The grid was perfectly dried and observed under the TEM at 150 kV.

2.6.4. Drug loading and encapsulation efficiency

To evaluate the drug concentration in a nanoparticle, a UV absorption measurement was performed. First, 3 mg of the nanoparticle was re-dissolved in 50 μL of acetone (spectroscopy grade), vortexed carefully with the final volume reaching 5 mL by adding phosphate buffered saline (PBS). Next, the insoluble magnetite debris was removed from the solution by centrifuging at 13,000 g for 15 min. Finally, the eupatorin content in the acetone solution was assessed by UV absorption at a maximum wavelength of 335 nm (characteristic absorption band of eupatorin). With respect to a standard plot of eupatorin calibration curve under the identical concentration, the amounts of drug content and encapsulated drug in the nanoparticle were calculated using Eqs. (1) and (2), respectively:

$$\text{Drug loading content }(\%) = \frac{\text{Weight of the eupatorin in nanoparticles}}{\text{Weight of nanoparticles}} \times 100 \quad (1)$$

$$\text{Encapsulation efficiency }(\%) = \frac{\text{Weight of the eupatorin in nanoparticles}}{\text{Weight of feeding eupatorin}} \times 100 \quad (2)$$

2.6.5. In vitro drug release

To study the drug release pattern, 3 mg of the nanoparticles were dispersed in 1 mL of PBS (pH = 7.4) and transferred into a pre-swelled dialysis bag (molecular weight cut-off 12,400 Da). Both

ends of the tube were fixed with a knot. The bag was immersed into the 10 mL of preheated PBS as a release medium with a similar pH to the PBS in the bag. Subsequently, beakers were placed on a stirrer whose temperature was set at 37 °C. At the selected time points, i.e., 1, 2, 4, 8, 24, 48, 72 and 200 h, 2 mL of the exterior solution was taken for UV–Vis analysis and replaced with 2 mL of fresh PBS. At fixed time intervals (e.g., 10 days) the medium in the vessel was completely removed and replaced with fresh release medium. The eupatorin concentration was determined by a UV–Vis spectrophotometer at maximum wavelength. According to the drug release behavior, the cumulative amount of released drug was calculated and the percentages of the released drug from mPEG-b-PLGA nanoparticles were plotted against time.

2.7. MTT assays of cell growth/viability

DU-145 and LNCaP cells were seeded in 96-well culture plates at a density of 10^4 cells/well. After overnight incubation, the medium was replaced with different doses of eupatorin and eupatorin-loaded Fe_3O_4@mPEG-b-PLGA nanoparticles (25—300 μM) for 24 h.

Stock solutions of eupatorin were prepared in dimethyl sulfoxide (DMSO) and were brought to different concentrations (5—300 μM) by dilution in medium immediately before use. The final concentration of the vehicle in the medium was always 0.1%.

The concentrations of eupatorin-loaded Fe_3O_4@mPEG-b-PLGA nanoparticles were calculated as equal to free eupatorin for comparing cell viability in the same doses. Since the evidence from drug release profiles showed that during the initial 24 h, around 30% of eupatorin was released from the nanoparticles, the desired amounts of eupatorin-loaded Fe_3O_4@mPEG-b-PLGA nanoparticles were weighted and dissolved in cell culture media. Each sample was vortexed for 30 min before treatment.

The viability of cells was determined by the MTT assay. Briefly, at the appropriate time, 20 μL of 5 mg/mL MTT was added to each well. The cells were incubated at 37 °C for 3 h and the medium was taken away and the purple formazan crystals were solubilized with 100 μL of DMSO. The absorbance was measured at 490 nm by a microplate reader (BioTek, ELX 800, USA). The results were expressed as the percentage of cell growth relative to the control untreated cells according to the following equation:

$$IC50 = (0.5 - b)/a \quad (3)$$

where a is the coefficient of concentration (slope of the line) and b is the intercept. These factors were obtained from the scatter plot of dose-response data.

2.8. Morphological analysis of the cell by Hoechst and Dil staining

For evaluating DNA condensation, DU-145 and LNCaP cells were seeded in 6-well culture plates at a density of 10^5 cells/well and treated with free eupatorin and eupatorin-loaded Fe_3O_4@mPEG-b-PLGA nanoparticles. After 24 h, both floating and attached cells were harvested and washed with PBS twice. The samples were fixed with cold methanol and kept at 4 °C overnight. The cells were added to the Hoechst solution 33342 with a concentration of 10 ng/mL and incubated for 10 min in the dark. They were then washed three times with PBS; DNA condensation and nuclear fragmentation were shown under the fluorescence microscopy (Zeiss, Germany). Dil is a fluorescent membrane dye for studying plasma membrane morphology. After drug treatment, the cells were

washed twice with PBS and exposed to Dil (20 μM) for 30 min in an incubator and then washed three times with PBS again. Plasma membrane morphologies were evaluated by fluorescence microscopy (Zeiss, Germany).

2.9. Cell cycle analysis

DU-145 and LNCaP cells were plated in 6-well culture dishes (3×10^5 per well). After preincubation, the cells were treated with the indicated concentration of free eupatorin and eupatorin-loaded Fe_3O_4@mPEG-b-PLGA nanoparticles for 24 h. After the treatment, both floating and attached cells were harvested, centrifuged and fixed for 3 h in 70% cold ethanol. After washing twice with cold PBS, the cells were re-suspended in PI Master Mix: 40 μL of propidium iodide (PI) (20 μg/mL), 950 μL of PBS and 10 μL of RNase (50 μg/mL) at 37 °C for 30 min in the dark. Cell cycle distribution was analyzed by flow cytometry (Coulter Epics Beckman, Germany). The resulting DNA was quantified by FlowJo software V7.6.1 (Developed by FlowJo LLC, Ashland, Oregon, USA) for detecting the sub-G1 phases of the cell cycle.

2.10. Annexin/PI cell death assay

To quantify apoptosis, DU-145 and LNCaP cells were seeded into 6-well plates with a density of 3×10^5 cells per well. After pre-incubation, the cells were treated with the indicated concentration of free eupatorin and eupatorin-loaded Fe_3O_4@mPEG-b-PLGA nanoparticles for 24 h. After the treatment, both floating and attached cells were collected, centrifuged and washed twice with PBS. The pellet was re-suspended in a mixture of 1X binding buffer (400 μL), PI (10 μL), and annexin V-FITC (5 μL). The mixture was incubated for 15 min in the dark at room temperature. The stained cells were analyzed directly by a flow cytometer (Coulter Epics, Beckman Coulter, Germany).

2.11. Nitric oxide release

To stimulate NO production, the Griess reagent (sulfanilamide and NED) under acidic conditions was used. Under this condition, the accumulated nitrite (NO_2^-), which is a stable breakdown product of NO, can be evaluated. After treatment of the cells, 50 μL of each condition medium was mixed with 50 μL of sulfanilamide solution and incubated for 10 min at room temperature in the dark. Then, 50 μL of NED was added to the mixture and shaken for 10 min in the dark. The absorbance was determined using the Biotek ELX800 microplate reader at 490 nm.

2.12. Western blotting

Detection of Bax/Bcl-2 ratio and cleaved caspase-3 in the cells extracts was determined by Western blotting analysis. After the treatment, cells were lysed in lysis buffer. Cells extracts were then harvested and the total protein concentrations were measured by Bradford's method [29]. Equal amounts of protein were electrophoresed by 12.5% SDS-PAGE gel and then transferred onto a PVDF membrane using a semi-dry transfer technique. Following the blocking stage with 5% non-fat dry milk in tris-buffered saline with Tween 20 (TBST), the membrane was probed with primary and secondary antibodies. Finally, the antibody-protein complexes were observed with an ECL detection kit (Amersham Bioscience, USA). Finally, the intensity of each band was measured using ImageJ (version 1.46).

2.13. Statistical analysis

The quantitative data were presented as mean ± SEM. A comparison between the groups was made by one-way analysis of variance (ANOVA), followed by Tukey's post hoc test to analyze the differences. The statistical significance was achieved with *P* values less than 0.05 (*$P < 0.05$, **$P < 0.01$, and ***$P < 0.001$).

3. Results

3.1. Identification of eupatorin

Eupatorin was obtained as yellow crystals, and its ^{1}H NMR (Fig. 1A), ^{13}C NMR (Fig. 1B), distortionless enhancement by polarization transfer (DEPT-135) (Fig. 1C) data were used to identify it as 5,3′-dihydroxy-6,7,4′-trimethoxyflavone. Its spectral data were in agreement with those previously described in the literature [25].

Eupatorin: ^{1}H NMR (500 MHz, $CDCl_3$, δ, ppm, *J*/Hz): 7.52 (1H, d, $J = 2.2$, H-2′), 7.48 (1H, dd, $J = 8.5, 2.2$, H-6′), 6.99 (1H, d, $J = 8.5$, H-5′), 6.62 (1H, s, H-8), 6.59 (1H, s, H-3), 4.03 (3H, s, OMe), 4.01 (3H, s, OMe), 3.97 (3H, s, OMe); ^{13}C NMR (125 MHz, $CDCl_3$, δ, ppm): 164.2s (C-2), 104.9d (C-3), 183.1s (C-4), 153.6s (C-5), 133.0s (C-6), 159.1s (C-7), 91.0d (C-8), 153.4s (C-9), 106.6s (C-10), 124.9s (C-1′), 111.1d (C-2′), 146.5s (C-3′), 149.9s (C-4′), 112.7d (C-5′), 119.5d (C-6′), 61.3q (OMe), 56.7q (OMe), 56.6q (OMe).

3.2. Preparation and characterization of nanoparticles

In this study, eupatorin-loaded Fe_3O_4@mPEG-b-PLGA nanoparticles were prepared, as described previously.

The size distribution of nanoparticles in drug delivery system is very important because of its impact on the drug release profile [30]. The mean particle size and distribution, as well as the zeta potential of the eupatorin-loaded Fe_3O_4@mPEG-b-PLGA nanoparticles were determined by a DLS technique using a Zetasizer Nano-ZS. According to the results of the DLS study, nanoparticles had a mean diameter of (58.5 ± 4) nm with polydispersity index of 0.167 ± 0.04. We verified that the nanoparticles had a uniform size and were well dispersed. The zeta potential of nanoparticles was found to be (-34.16 ± 1.3) mV, suggesting the sufficiently high surface charge of the nanoparticles and confirming their stability in dispersion [31].

TGA is a useful method for the determination of the residual components in nanoparticles and is based on the observation of weight loss of individual components. As shown in Fig. 2A, 6% weight loss in the TGA curve (a) corresponds to the removal of absorbed water in Fe_3O_4 nanoparticles. The second peak (b) represents the oleic acid-stabilized Fe_3O_4 nanoparticles and the weight loss is also associated with the evaporation of water and decomposition of oleic acid. The third peak (c) shows Fe_3O_4@mPEG-b-PLGA nanoparticles and the weight loss is related to the degradation of the mPEG-b-PLGA layer in the range of 200–400 °C. The maximum weight loss temperature is about 300 °C according to the differential thermogravimetric (DTG) thermogram (Fig. 2B) and the percentage of the weight loss is 33.62 % (*m/V*). The residual weight of the sample above 300 °C indicates that only Fe_3O_4 nanoparticles remained and the mPEG-b-PLGA had been completely decomposed. These results suggest that most of the initial magnetite nanoparticles were incorporated into the mPEG-b-PLGA polymer matrix.

Nanoparticle morphological features were analyzed with TEM. As shown in Fig. 3A, TEM image verified that most of the
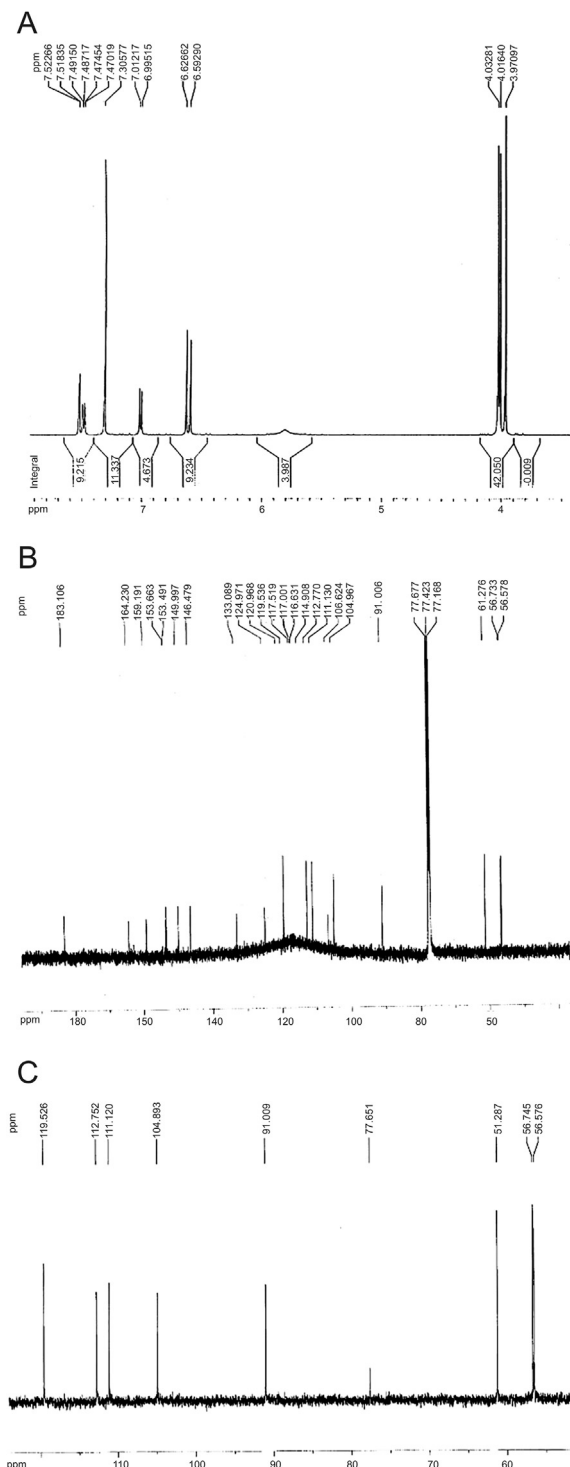
Fig. 1. Identification of eupatorin. (A) ^{1}H NMR (CDCl$_3$, 500 MHz). (B) ^{13}C NMR (CDCl$_3$, 125 MHz) and (C) DEPT-135 NMR (CDCl$_3$, 125 MHz) spectrum of eupatorin.

nanoparticles had a regular spherical shape, and at optimum conditions, the particle size was below 100 nm. Dark regions correspond to the magnetic nanoparticles incorporated into the mPEG-b-PLGA domains. The results suggest that the magnetic nanoparticles are well coated with the mPEG-b-PLGA. SAED patterns of nanoparticles are presented in Fig. 3B. The presence of white spotty

diffraction rings attributed to the (220), (311), (400), (422), (511), and (440) planes of the cubic inverse spinel construction of the magnetite was indicated using the SAED pattern, demonstrating the presence of SPION nanoparticles.

3.2.1. Drug content and encapsulation efficiency of nanoparticles

Eupatorin-loaded Fe$_3$O$_4$@mPEG-b-PLGA nanoparticles were quantified for their drug loading percentage and encapsulation efficiency by absorption spectra at 335 nm using calibration curve which was generated by known concentrations of eupatorin solutions. The drug content and encapsulation efficiency of the nanoparticles were (8.28 ± 0.14)% and (90.99 ± 2.1)%, respectively.

3.2.2. In vitro drug release

In order to determine whether eupatorin-loaded Fe$_3$O$_4$@mPEG-b-PLGA nanoparticles are effective in drug delivery, we employed the in vitro drug release of eupatorin from nanoparticles at different time intervals (1, 2, 4, 8, 24, 48, 72 and 200 h). Our findings showed that eupatorin was initially released at a rapid rate with 30% of it released in 24 h, which was followed by the gradual release until 200 h (Fig. 4). The observed burst release could be due to the release of the absorbed eupatorin on the surface of nanoparticle whereas the sustained release was attributed to the release of the encapsulated eupatorin from the polymer matrix.

3.3. Effects of free eupatorin and eupatorin-loaded Fe$_3$O$_4$@mPEG-b-PLGA nanoparticles on the cell growth

The cell growth rate was assessed in the presence of various concentrations of free eupatorin and eupatorin-loaded Fe$_3$O$_4$@m-PEG-b-PLGA nanoparticles (25—300 μM) using MTT assay. The results showed that the viability of both human prostate cancer cell lines was decreased in a dose-dependent manner in 24 h.

In DU-145 cells, the IC50 values of the free eupatorin and eupatorin-loaded Fe$_3$O$_4$@mPEG-b-PLGA nanoparticles were 150 μM and 100 μM (Fig. 5A) while in LNCaPs they were 100 μM and 75 μM, respectively (Fig. 5B). It was also demonstrated that the blank nanoparticles (Fe$_3$O$_4$@mPEG-b-PLGA nanoparticles) and DMSO as the eupatorin solvent had no significant effects on the growth rate of either of the cell lines. On the other hand, free eupatorin and eupatorin-loaded Fe$_3$O$_4$@mPEG-b-PLGA nanoparticles displayed negligible toxicity against HUVECs as normal cells (Fig. 5C). These results indicated that the slower and sustained release of eupatorin from the nanoparticles reduced its effective dose (IC50) and showed better in vitro therapeutic effects than free eupatorin in both prostate cell lines.

After MTT assay, the IC50 of eupatorin-loaded Fe$_3$O$_4$@mPEG-b-PLGA nanoparticles (100 μM for DU-145 and 75 μM for LNCaP) was determined for all treatments and 3 groups were defined for each cell lines: control, free eupatorin, and nano-eupatorin.

3.4. Morphological analysis of apoptotic cells by fluorescence staining

Apoptosis includes a collection of biochemical events leading to many types of morphological changes, such as cell blebbing, cell lysis, plasma membrane changes, cell shrinkage, nuclear fragmentation, chromatin condensation and DNA degradation [32]. Change in nuclear morphology is proof of the late stage in cell apoptosis with the change in Hoechst staining intensity [33]. As shown in Fig. 6, untreated cells displayed pseudopodial projections with prominent nuclei and intact cell membranes. Free eupatorin and nano-eupatorin induced morphological modifications and nuclear condensation in both DU-145 (Fig. 6B and C) and LNCaP (Fig. 6E and F) cells when compared with the control (Fig. 6A and D). However,
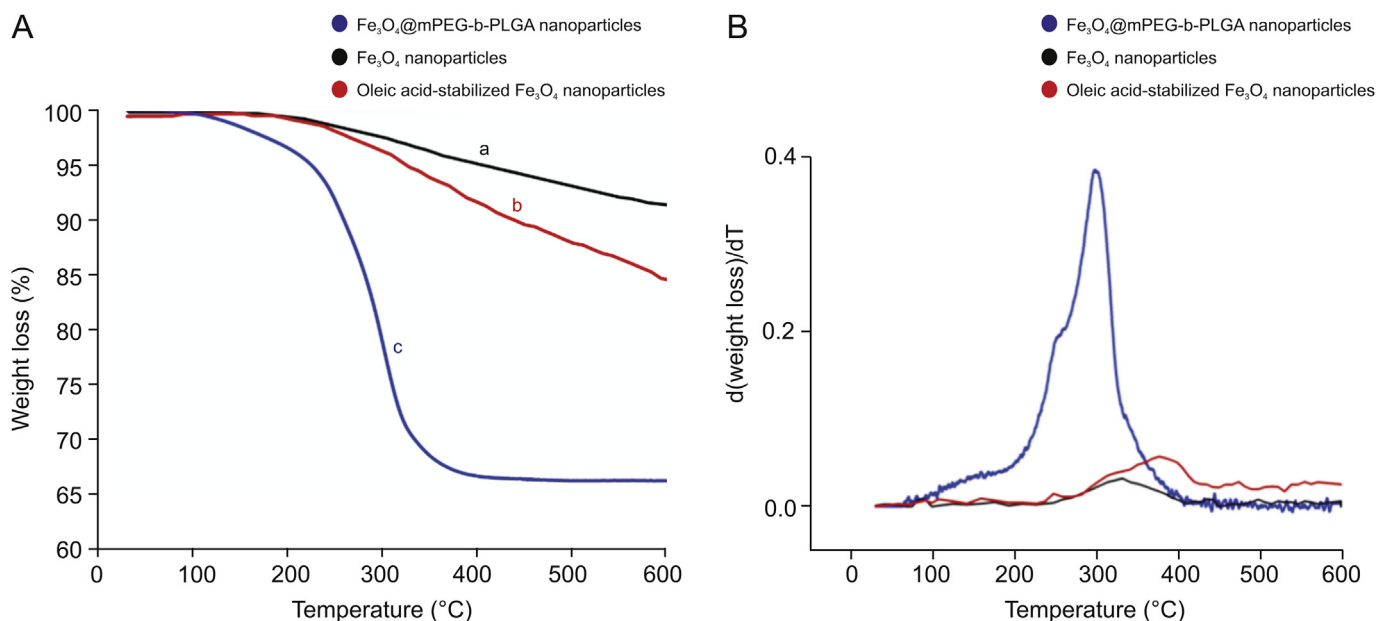
Fig. 2. Thermal gravimetric analysis/differential thermogravimetric (TGA/DTG) of nanoparticles. (A) TGA curves of Fe_3O_4 nanoparticle (a-black), oleic acid-stabilized Fe_3O_4 nanoparticles (b-red) and Fe_3O_4@mPEG-b-PLGA nanoparticles (c-blue). (B) Corresponding DTG thermogram.
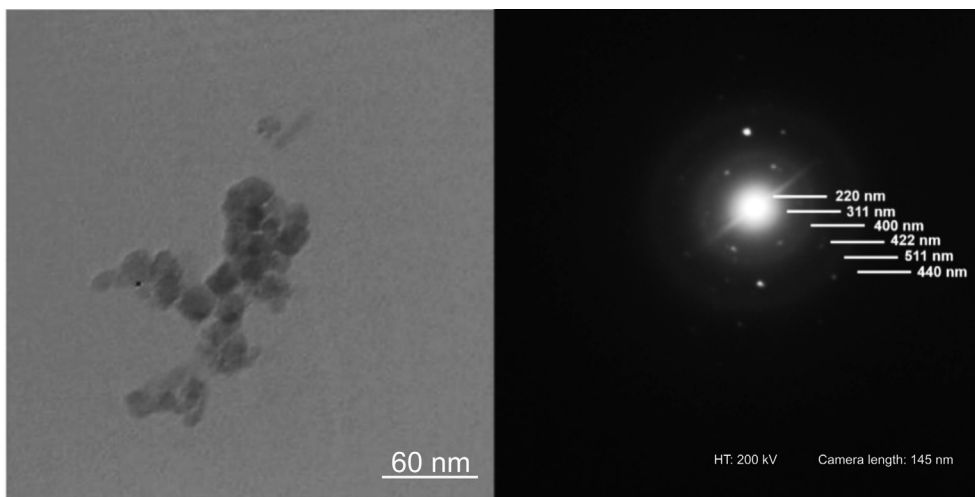
Fig. 3. TEM micrographs of eupatorin-loaded Fe_3O_4@mPEG-b-PLGA nanoparticles. The TEM image revealed the smooth spherical shape of nanoparticles with good dispersibility (Magnification bar = 60 nm).

the apoptotic index for the cells treated with nano-eupatorin was significantly increased and the cells displayed crescent-shaped nuclei with compact chromatin (arrows). In addition, obvious reductions in the total cell numbers and morphological changes occurred simultaneously because of the anti-proliferative activity of eupatorin.

Dil stain was used for detecting plasma membrane morphology. It is softly fluorescent in aqueous suspension, but becomes bright when bound to the cell membrane and diffuses laterally to the entire cell. As can be seen in Fig. 6, treatment with nano-eupatorin, compared to free eupatorin, was more effective in making the cells non-adherent and round shaped (arrowheads) in both DU-145 (Fig. 6H and I) and LNCaP (Fig. 6K and L) cell lines in comparison

with the control cells.

3.5. Effect of free eupatorin and nano-eupatorin on cell cycle

The flow cytometric analysis was used in order to determine how free eupatorin and nano-eupatorin had changed the distribution of cells during cell cycle phases. Free eupatorin induced an arrest of cells at the G2-M interphase in both cell lines, for DU-145: 38.14% (Fig. 7B) compared with control 20.38% (Fig. 7A) and for LNCaP: 31.63% (Fig. 7E) compared with control 15.93% (Fig. 7D). Interestingly, free eupatorin did not significantly affect the cells in the S and sub G1 phases. In contrast, treatment of the cells with nano-eupatorin led to a further increase in sub-G1 arrest in both
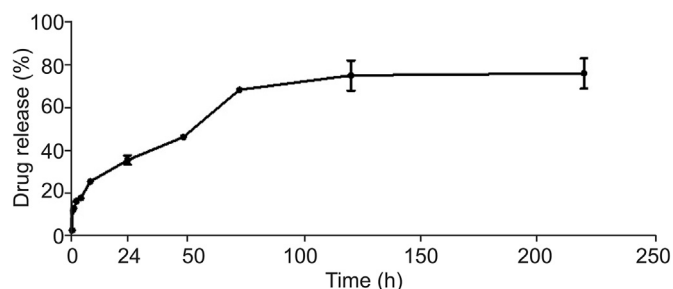
Fig. 4. In vitro release profile of eupatorin-loaded Fe$_3$O$_4$@mPEG-b-PLGA nanoparticles in PBS buffer (pH 7.4) at 37 °C. The release curve showed the burst release phase and sustained release phase. About 30% of the eupatorin was released during the first 24 h as a burst release phase. The sustained release phase started after the first 24 h and continued to 200 h during which the amount of release reached approximately 80%. The plot represents the mean ± SD of triplicate results.

cell lines, for DU-145: 20.33% (Fig. 7C) compared with control 2% (Fig. 7A) and for LNCaP: 12.43% (Fig. 7F) compared with control 1.7% (Fig. 7D). Using the percentage of cells in the sub-G1 peak as a marker for apoptosis due to DNA fragmentation [34], apoptosis was verified in DU-145 and LNCaP human prostate cancer cell lines during nano-eupatorin treatment.

3.6. The effect of eupatorin and nano-eupatorin on the induction of apoptosis

The annexin V-PI assay is based on the principle that just after the induction of apoptosis, phosphatidylserine is displaced from the inner plasma membrane to the outer leaflet [35]. The binding of annexin V to phosphatidylserine (PS) and PI to nucleic acids can be used to detect the population of apoptotic cells. Free eupatorin had the same effects on DU-145 and LNCaP human prostate cancer cell lines and increased both necrotic and late apoptotic cells (Figs. 8B and E) compared to the untreated group (Figs. 8A and D). As shown in Fig. 8C, although nano-eupatorin showed the same effects as that of free eupatorin on DU-145 apoptosis rate (11% apoptosis by free eupatorin vs. 16% apoptosis by nano-eupatorin), it could significantly reduce the necrotic cells (12% necrosis by free eupatorin vs. 4% necrosis by nano-eupatorin). On the other hand, in LNCaP cells, necrosis and late apoptosis rate had no significant change following nano- and free eupatorin treatment (Figs. 8E and F). However, as shown in Fig. 8F, nano-eupatorin was more effective in comparison to free eupatorin in increasing the number of cells undergoing early apoptosis (3% early apoptosis by free eupatorin vs. 40% early apoptosis by nano-eupatorin).

3.7. Comparison of NO production between free eupatorin and nano-eupatorin

Evaluation of nitrite accumulation in the culture medium was used to specify NO production. Cells were treated as described previously and the culture medium was gathered after 24 h incubation. The nitrite concentration was measured by Griess reagent. As shown in Fig. 9, nano-eupatorin, in comparison with the control group, significantly increased NO production in both DU-145 (1.4 fold) and LNCaP (2.8 fold) cell lines while no significant changes were observed in the free eupatorin treated group.

3.8. Free eupatorin and nano-eupatorin changed the expression level of apoptotic-related proteins

Two main groups of proteins that play an important role in

apoptotic cell death are the members of the Bcl-2 family and a class of cysteine proteases known as caspases [36]. The Bcl-2 family can be divided into two functionally separate groups: anti-apoptotic proteins and pro-apoptotic proteins. Bcl-2 is an anti-apoptotic protein and protects against cell death. Bax is a pro-apoptotic protein that is expressed during apoptosis and promotes cell death. Increasing Bax/Bcl-2 ratio has commonly been used to show the induction of apoptosis in cells [37]. Western blotting was applied to assess the expressions of Bcl-2, Bax, and caspase-3 (Fig. 10A). As shown in Fig. 10B, in cells treated with free eupatorin, Bax/Bcl-2 ratios were increased to 5.1 and 7.5 in DU-145 and LNCaP cells, respectively. Interestingly, nano-eupatorin was significantly more effective than its free form and increased Bax/Bcl-2 ratio to 13.5 and 20.5 in DU-145 and LNCaP, respectively, in comparison with the control. Furthermore, nano-eupatorin increased the levels of cleaved caspase-3 to 2.5 fold and 1.7 fold in DU-145s and LNCaPs, respectively (Fig. 10C). Finally, no significant difference was observed in cleaved caspase-3 levels in the free eupatorin treated cells vs. control group.

4. Discussion

Today, cancer is a great danger and affects the lives of millions of people all over the world. Although much money is spent in developing chemotherapy drugs and treatment methods each year, most patients suffer from serious unwanted side effects due to the non-selective effects of chemotherapeutic drugs on normal cells [38]. Phytochemicals, the bioactive compounds in fruits, vegetables, nuts, seeds, plants, and marine products have been linked to reducing the incidence of major diseases including cancer by inducing apoptosis, autophagy and inhibiting cell proliferation [39].

Among multiple plant-based bioactive compounds, flavonoids have been well described. They are classified into six groups: flavonols, flavones, flavanols, flavanones, anthocyanidins, and isoflavonoids. Eupatorin (C$_{18}$H$_{16}$O$_7$/3′,5-dihydroxy-4′,6,7-trimethoxyflavone) is one of the powerful flavonoid candidates which suppresses proliferation and induces apoptosis in multiple cancer cellular models [40]. The therapeutic efficacy of eupatorin is greatly limited by the low solubility, poor permeability, low bioavailability and short biological half-life [41].

Various nanocarriers are reported in the literature for their drug delivery system, which bypass such limitations in cancer treatment [42]. In this study, we designed the encapsulation of eupatorin in mPEG-b-PLGA coated iron oxide nanoparticle as a carrier to compare the inhibitory effects of the free and nano-forms of eupatorin on cell proliferation in human prostate cancer cellular models. SPIONs which consist of magnetite (Fe$_3$O$_4$) have quickly become promising candidates for cancer therapy because of their high magnetic responsiveness, biodegradability, biocompatibility and high delivery efficiency [43]. Also, several studies have reported that SPIONs are widely used as magnetic resonance imaging contrast agents for the prediction and real-time monitoring of anticancer drug release in vitro and in vivo [44]. In this study, Fe$_3$O$_4$ nanoparticles were stabilized by oleic acid in order to improve SPIONs with better oil-solubility, stability, and low cytotoxicity. As naked SPIONs can easily aggregate and precipitate in aqueous solutions and blood plasma [45], we coated SPIONs with the mPEG-b-PLGA polymer to increase nanoparticles' biocompatibility and uptake by the cells. PLGA is a well-known biocompatible polymer, which is hydrolytically degraded into nontoxic oligomers and monomers, lactic acid and glycolic acid. It has been extensively engaged in the applications of drug delivery, tissue engineering and molecular imaging [46].

The results showed that most of the synthesized nanoparticles had a uniform spherical shape, optimum size and were well dispersed. The surface zeta potential of the eupatorin-loaded
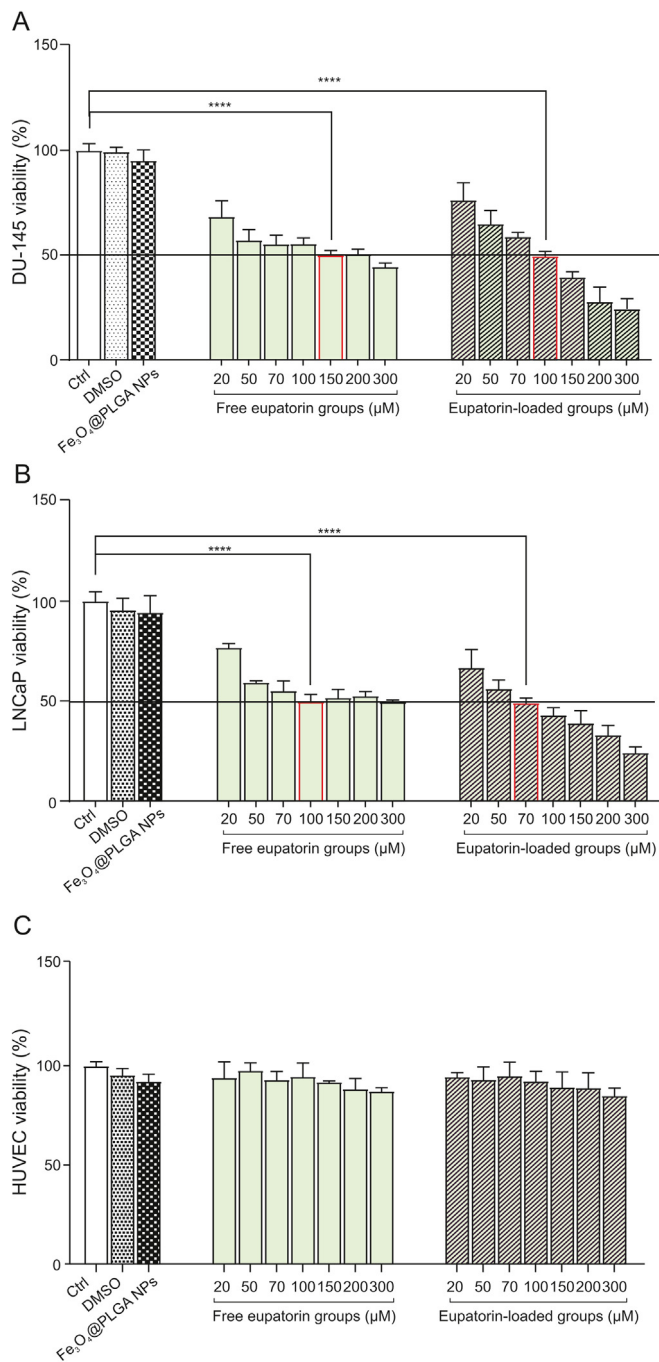
Fig. 5. Inhibitory effect of free eupatorin, eupatorin-loaded Fe_3O_4@mPEG-b-PLGA nanoparticles and Fe_3O_4@mPEG-b-PLGA nanoparticles on cell viability in DU-145 cells (A), LNCaP cells (B) and HUVEC cells (C) after 24 h. Although there was a reduction in viability of DU-145 and LNCaP cells treated with both forms of eupatorin in comparison with control, eupatorin-loaded Fe_3O_4@mPEG-b-PLGA nanoparticles reduced IC50 dose from 150 μM to 100 μM in DU-145 and from 100 μM to 75 μM in LNCaP cells, in comparison with free eupatorin treatment. HUVECs as normal cells showed no significant reduction in viability. It was also demonstrated that the blank nanoparticles and DMSO, at the dose which was equal to the highest concentration of eupatorin, had no significant effects on the growth rate of either of the cell lines. All data are presented as mean ± SD ($n = 7$). The significant difference was found by one-way ANOVA, compared to the untreated control. ****$P < 0.0001$. DMSO: dimethyl sulfoxide; NP: nanoparticle.

Fe_3O_4@mPEG-b-PLGA nanoparticles was (-34.16 ± 1.3) mV. This negative charge was enough to make the particles repel each other, therefore preventing the possibility of aggregation and remaining in circulation for a long time. The drug release behavior from the nanoparticles exhibited a biphasic pattern with the initial burst release, followed by a lag period of about 200 h (Fig. 4). The sustained release of the entrapped drug from the nanoparticles prolonged the biological half-life of the natural compounds in the

plasma [47].

Cancer cells are highly metabolic and porous in nature and are known to internalize nanoparticles rapidly, compared to the normal cells, through enhanced permeability [48]. Therefore, we hypothesized that eupatorin-loaded Fe_3O_4@mPEG-b-PLGA nanoparticles will uptake within both prostate cancer cell lines and release their payload after entering the cell.

The in vitro cell growth/viability test (MTT assay) was performed
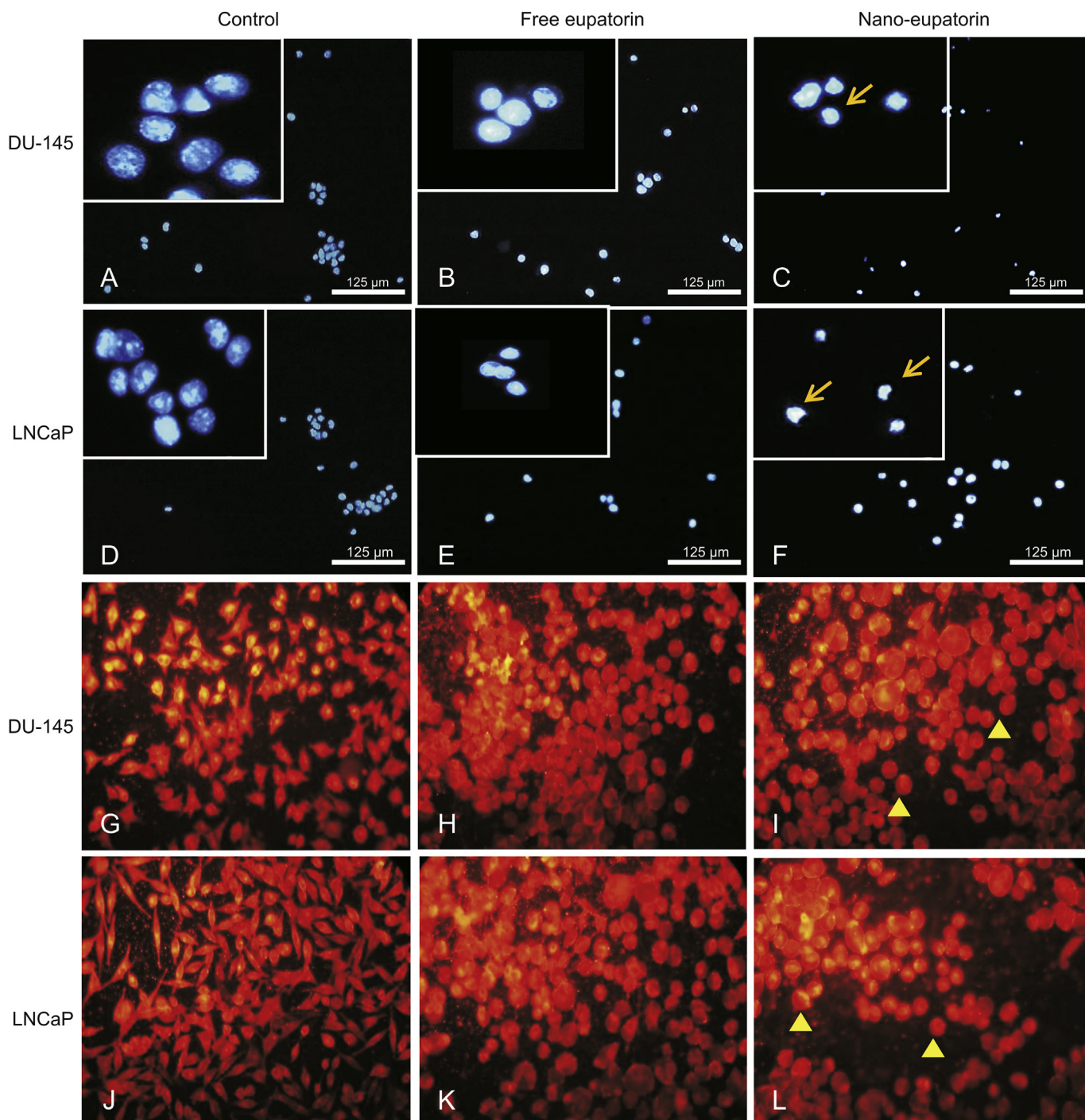
Fig. 6. Hoechst and Dil staining. The cells were treated with the IC50 of eupatorin-loaded Fe$_3$O$_4$@mPEG–b–PLGA nanoparticles (100 μM for DU-145 and 75 μM for LNCaP) for 24 h. Nuclear morphology and plasma membrane changes of apoptotic cells can be investigated by phase-contrast fluorescence microscopic examination. Free eupatorin induced nuclear condensation in both DU-145 (B) and LNCaP (E) cells. However, as identified by the arrows, the apoptotic index for the cells treated with nano-eupatorin was significantly increased and crescent-shaped nuclei with compact chromatin were seen in both DU-145 (C) and LNCaP (F) cells in comparison with the control (A and D). Similarly, treatment with nano-eupatorin, compared to free form, was more effective in making the cells round shaped in both DU-145s (H and I) and LNCaPs (K and L), in comparison with the control cells (G and J). Arrowheads display a reduction in cell adhesion of apoptotic cells. All experiments were repeated three times.

to evaluate the effects of both free and nano-forms of eupatorin against two prostate cancer cell lines (DU-145 and LNCaP). The results showed that although there is a decrease in the viability of both cell lines up to 50 μM of free eupatorin, dose-dependent increase up to 300 μM makes no significant change on cells' viability. In contrast, by using nano-eupatorin, a decreased cell growth rate

was detected, which suggested that nano-encapsulation protects eupatorin against degradation and enhances its biocompatibility and solubilization potential. In our study, high encapsulation efficiency (90.00%) provides optimal drug loading of nanoparticles and thus increases the therapeutic index and decreases the effective dose of eupatorin. In another study by Nassir et al., [49] resveratrol
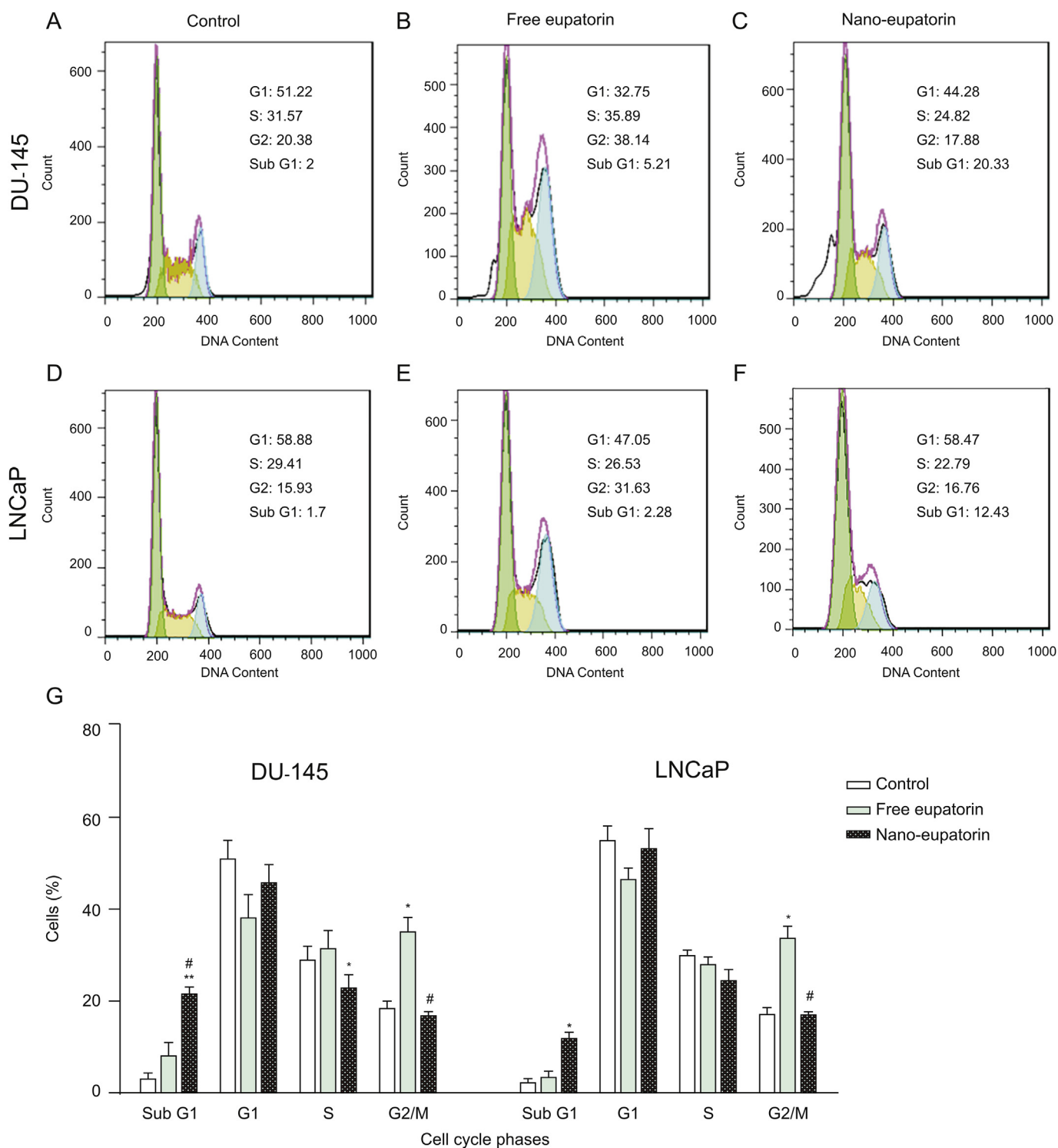
Fig. 7. Cell cycle arrest. DU-145 and LNCaP cells were incubated in the presence of the IC50 of eupatorin-loaded Fe_3O_4@mPEG-b-PLGA nanoparticles (100 μM for DU-145 and 75 μM for LNCaP) for 24 h. The cell cycle phase distribution was determined by flow cytometry and graphs A to E represent one of the replicates. Interestingly, although free eupatorin induced an arrest of cells at the G2/M interphase in both DU-145 and LNCaP cells (B and E), it did not significantly affect the cells in the S and sub G1 phases. In contrast, treatment of the cells with nano-eupatorin led to a further increase in sub-G1 arrest in both DU-145 (C) and LNCaP cells (F) compared with control (A and D). A summary of cell cycle progression has been shown in bar graph (G). Data are shown as the mean ± standard deviation ($n = 3$). *Significantly different from control cells (*$P < 0.05$, **$P < 0.01$). [#] Significantly different from free eupatorin ([#]$P < 0.05$).
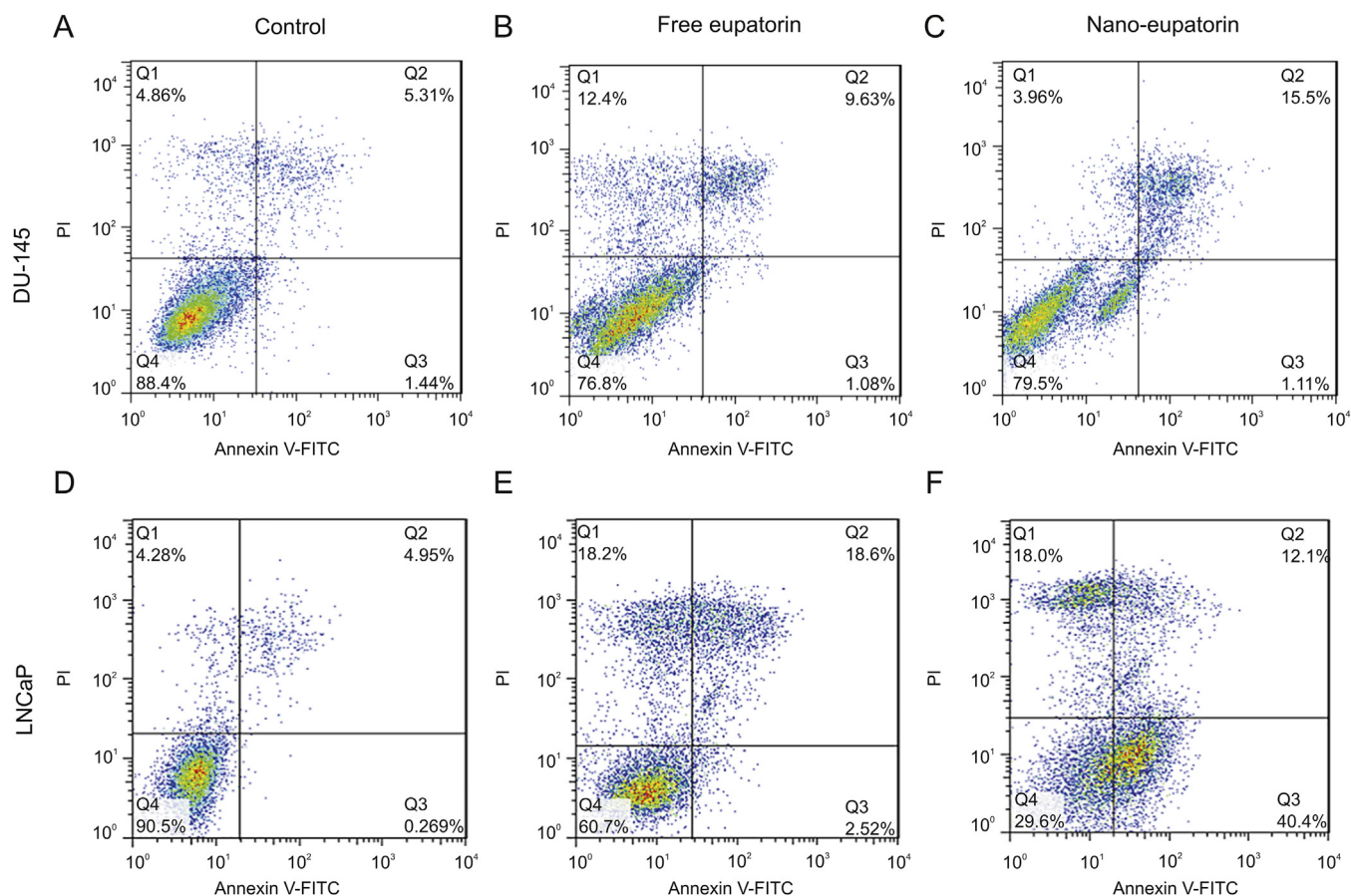
Fig. 8. Apoptosis percentage. Detection of apoptotic cells by annexin V-FITC and propidium iodide-doubled staining after treatment with the IC50 dose of eupatorin-loaded Fe$_3$O$_4$@mPEG-b-PLGA nanoparticles (100 μM for DU-145 and 75 μM for LNCaP) for 24 h. Q1 shows necrotic cells, Q2 shows late apoptotic cells, Q3 shows early apoptotic cells, and Q4 shows the viable cells. Free eupatorin had the same effects on both human prostate cancer cell lines and increased necrotic and late apoptotic cells (B and E) in comparison with control (A and D). Interestingly, although nano-eupatorin showed the same effects as that of free eupatorin on the DU-145 apoptosis rate, it could significantly reduce the necrotic cells (C). On the other hand, in LNCaP cells, necrosis and late apoptosis rate had no significant change following nano- and free eupatorin treatment (E and F). However, nano eupatorin was more effective in comparison to free form in increasing the number of cells undergoing early apoptosis. All experiments were repeated three times.

(RL), a natural polyphenol, and resveratrol-loaded PLGA nanoparticles (RLPLGA) were designed and their mode of apoptotic cells death against LNCaPs was determined. Similar to our findings, clear evidence for enhanced LNCaPs growth inhibition was observed for RLPLGA nanoparticles which exhibited an IC50 of 15.6 μM and IC90 of 41.1 μM, compared to RL which had nearly double IC50 and IC90. Also, the results of the MTT cell viability assay for the curcumin and curcumin-loaded PLGA nanoparticles on prostate cancer cell lines, LNCaP, PC3, DU145, and a nontumorigenic cell line (PWR1E) showed a 35% reduction in IC50 when curcumin was encapsulated in nanoparticles [50]. In addition, as an IC50 dose for both free and nano-forms of eupatorin in LNCaP cells is lower than DU-145 (100 μM vs. 150 μM in free and 75 μM vs. 100 μM in nano-form respectively), it can be suggested that androgen receptors (AR) in LNCaPs make them more capable than DU-145s of receiving the eupatorin released from the nanoparticles. Flavonoids are a group of phytoestrogens and have a structural similarity to testosterone [51] and have a binding affinity to AR [52]. Some possible mechanisms of flavonoid action on the AR in prostate cancer include competing with androgens for AR binding sites, induction of AR degradation and inhibition of ligand-AR complex translocation to the nucleus [53].

Manipulation of the cell cycle may either prevent or induce an apoptotic response in cells. Therefore, the cell cycle is known as one of the critical points in the treatment of cancer. Like many other flavonoids, eupatorin is able to inhibit the proliferation of cancer cells mainly by arresting cell cycle progression. Eupatorin is able to arrest cells at the G2-M phase in human leukemia cells [54], human colon cancer cells [55], HeLa cervical carcinoma cells [56] and MDA-MB-468 cells [8]. Eupatorin-5-methyl ether (C$_{19}$H$_{18}$O$_7$) caused G1 arrest in MCF7 cells and upregulation of p21, JNK, p-JNK [57]. Our results are similar to those of the literature described above and we observed that the IC50 dose of free eupatorin induced G2/M arrest in both cell lines while the IC50 concentration of the nano-eupatorin caused subG1 arrest which might result in apoptosis induction. These findings are consistent with those of other studies which have demonstrated that cell cycle distribution in treatment with drug loaded nanoparticles may have a different effect compared to the free form of the drugs [58,59].

We have further analyzed the rate of apoptosis with annexin/PI thorough phosphatidylserine redistribution to confirm the results from the cell cycle. Our findings confirmed that eupatorin increased the percentage of apoptotic and necrotic cells in both DU-145 and LNCaP cell lines [55]. Although nano-eupatorin treatment induced approximately the same early and late apoptosis compared to its free form, the significant decrease in necrosis rate was observed in DU-145 cells. However, in LNCaP cells, nano-eupatorin had similar effects in inducing a late stage of apoptosis and necrosis but was more effective than free eupatorin in inducing the early stage of apoptosis. This finding is consistent with the study by Lin et al. [60],
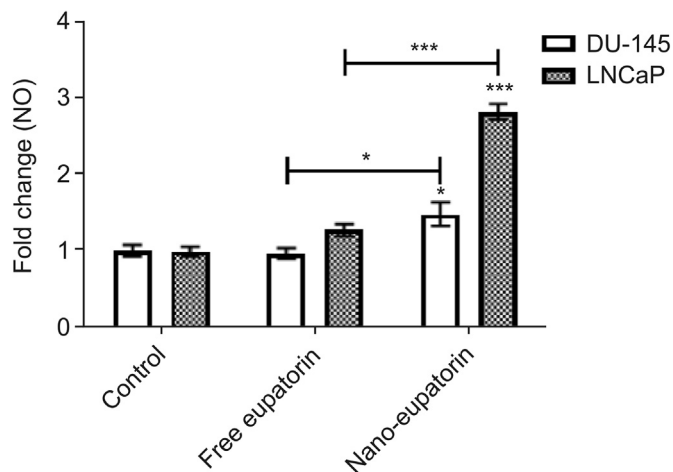
Fig. 9. Effect of the IC50 of eupatorin-loaded Fe$_3$O$_4$@mPEG-b-PLGA nanoparticles (100 μM for DU-145 and 75 μM for LNCaP) on NO production after 24 h. In comparison with the control group, nano-eupatorin significantly increased NO production in both DU-145 (1.4 fold) and LNCaP (2.8 fold) cell lines, while no significant change was observed in the free eupatorin treated group. The results are expressed as mean ± SEM ($n = 3$). *$P < 0.05$ and ***$P < 0.001$.

which showed that liposomal berberine could enhance early apoptosis in HepG2 cells compared to free berberine.

In the next step, the amount of NO, as an important mediator that participates in a variety of physiological and biological pathways associated with cell apoptosis and proliferation, was determined [61,62]. NO, a free radical and water-soluble gas produced endogenously, may demonstrate a biphasic response in tumor cells. At low concentrations (less than 100 nM), it causes angiogenesis which leads to tumor progression. On the contrary, at high concentrations (more than 500 nM), NO acts as a proapoptotic modulator and tends to be cytotoxic in cancer cells [63]. Interestingly, Laavola et al. [7] demonstrated that eupatorin had a biphasic effect on NO production. While at low concentrations, approximately 40 μM nitrite was produced by murine J774 macrophages, NO production was inhibited by eupatorin at high concentrations. This could be used to verify our results which showed that free eupatorin did not make any significant changes in NO production. On the other hand, sustained release of eupatorin in nano-formulated form can lead to a lower dose requirement, causing an overproduction of NO which initiates apoptotic pathways resulting in a remarkable anti-cancer effect on both human prostate cancer cell lines. Prolonged production of NO has been associated with the release of cytochrome C from the mitochondria, activation of caspase, modulation of anti-apoptotic Bcl-2 proteins, and increase in p53expression [64]. Also, activation of AR could lead to NO production [65] which inhibits the proliferation of AR-positive (LNCaP) much more efficiently than AR-negative (DU-145) human prostate cancer cells [66].

Our results confirmed that although the nano-form has a stronger effect, both the free and nano-forms of eupatorin increased the expression of Bax (a pro-apoptotic protein) and decreased the expression of Bcl-2 (an anti-apoptotic protein), leading to an increase in Bax/Bcl-2 ratio in DU-145 and LNCaP prostate cancer cells in comparison with untreated cells. This is in line with Sarvestani et al. [67] who reported that eupatorin induced apoptosis via the mitochondrial pathway by decreasing mitochondrial membrane potential and increasing the ratio of Bax/Bcl-2 expression. Interestingly, although there is no significant difference between free eupatorin and control, nano-eupatorin led to huge increases in the expression of cleaved caspase-3, especially in the
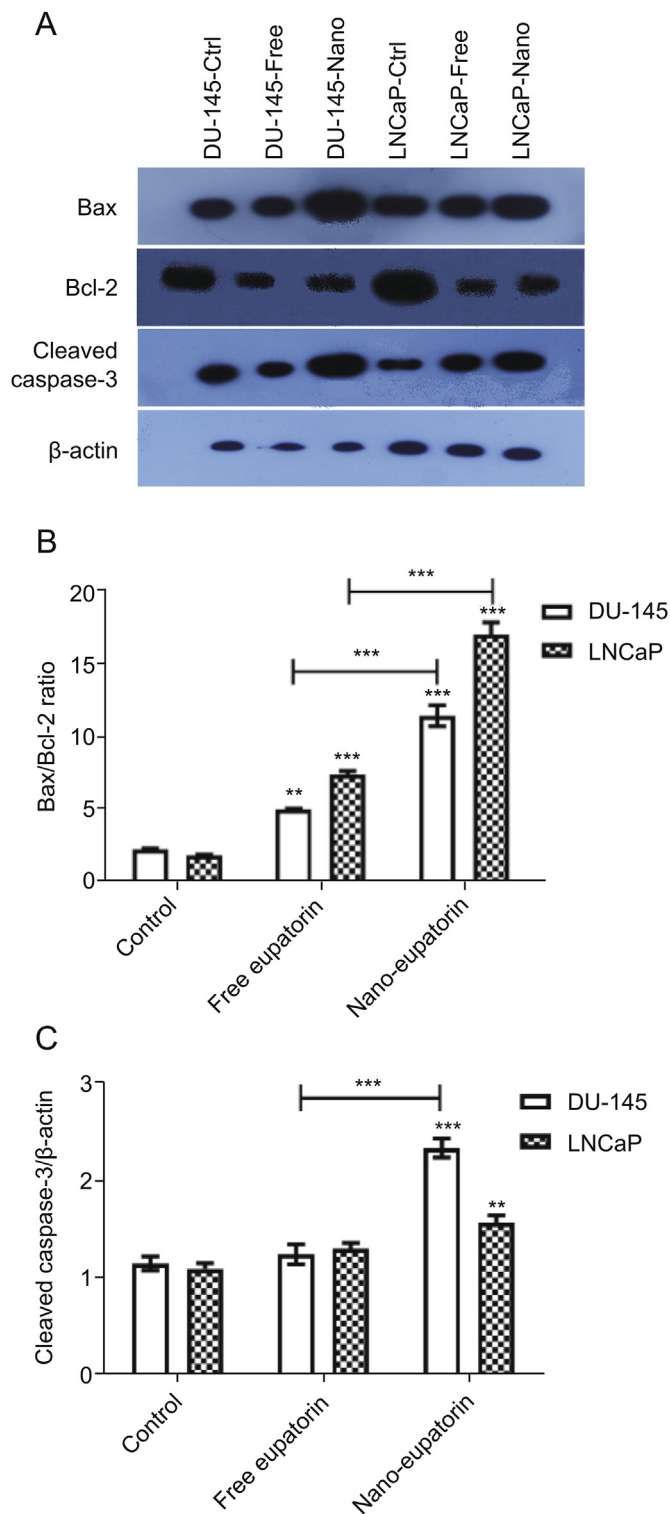
Fig. 10. Western blotting analysis of apoptotic proteins in human prostate cancer cell lines. Cells were treated with the indicated concentration of eupatorin-loaded Fe$_3$O$_4$@mPEG-b-PLGA nanoparticles (100 μM for DU-145 and 75 μM for LNCaP) for 24 h. Effect of free eupatorin and nano-eupatorin on the expression of Bax, Bcl-2, and cleaved caspase-3 levels (A). The densities of Bax/Bcl-2 ratio (B) and cleaved caspase-3 (C) bands were measured, and their ratio to β-actin was calculated. As noted above, nano-eupatorin was significantly more effective than its free form in increasing the Bax/Bcl-2 ratio and the levels of cleaved caspase-3 in DU-145 and LNCaP cells.

DU-145 cell line. This may be due to the fact that at the first stage of eupatorin release, apoptotic pathway is triggered from mitochondria by increasing the amounts of Bcl-2 family proteins. Since there is a lag time between translocation of Bax and cell death, sustained eupatorin release is able to shift cells at the end stage of apoptosis and increase the expression of cleaved caspase-3.

5. Conclusions

In conclusion, our results indicated that the treatment of DU-145 and LNCaP human prostate cancer cell lines with eupatorin-loaded Fe_3O_4@mPEG-b-PLGA nanoparticles can be more effective in inhibiting cancer cell growth in comparison to the treatment with free eupatorin. Based on these results, this formulation can provide a sustained release of eupatorin into tumor cells, which makes it a suitable candidate for pharmacological use. However, more animal models and in vivo studies are required to clarify the efficacy and safety of eupatorin-loaded Fe_3O_4@mPEG-b-PLGA nanoparticles before clinical trials in the future.

Declaration of competing interest

The authors declare that there are no conflicts of interest.

Acknowledgments

Appendix A. Supplementary data

Supplementary data to this article can be found online at https://doi.org/10.1016/j.jpha.2020.04.002.

References

[1] F. Bray, J. Ferlay, I. Soerjomataram, et al., Global cancer Statistics 2018: GLOBOCAN estimates of incidence and mortality worldwide for 36 cancers in 185 countries, CA A Cancer J. Clin. 68 (2018) 394–424.

[2] R. Chen, S. Ren, M.K. Yiu, et al., Prostate cancer in Asia: a collaborative report, Asian J. Urol. 1 (2014) 15–29.

[3] A. Rodriguez-Casado, The health potential of fruits and vegetables phytochemicals: notable examples, Crit. Rev. Food Sci. Nutr. 56 (2016) 1097–1107.

[4] D. Raffa, B. Maggio, M.V. Raimondi, et al., Recent discoveries of anticancer flavonoids, Eur. J. Med. Chem. 142 (2017) 213–228.

[5] I. Dolečková, L. Rárová, J. Grúz, et al., Antiproliferative and antiangiogenic effects of flavone eupatorin, an active constituent of chloroform extract of Orthosiphon stamineus leaves, Fitoterapia 83 (2012) 1000–1007.

[6] N.A. Razak, N. Abu, W.Y. Ho, et al., Cytotoxicity of eupatorin in MCF-7 and MDA-MB-231 human breast cancer cells via cell cycle arrest, antiangiogenesis and induction of apoptosis, Sci. Rep. 9 (2019), 1514.

[7] M. Laavola, R. Nieminen, M. Yam, et al., Flavonoids eupatorin and sinensetin present in Orthosiphon stamineus leaves inhibit inflammatory gene expression and STAT1 activation, Planta Med. 78 (2012) 779–786.

[8] V. Androutsopoulos, R.R.J. Arroo, J.F. Hall, et al., Antiproliferative and cytostatic effects of the natural product eupatorin on MDA-MB-468 human breast cancer cells due to CYP1-mediated metabolism, Breast Cancer Res. 10 (2008), R39.

[9] V. Sanna, I.a. Siddiqui, M. Sechi, et al., Nanoformulation of natural products for prevention and therapy of prostate cancer, Canc. Lett. 334 (2013) 142–151.

[10] I.A. Siddiqui, V. Sanna, Impact of nanotechnology on the delivery of natural products for cancer prevention and therapy, Mol. Nutr. Food Res. 60 (2016) 1330–1341.

[11] D. Kashyap, H.S. Tuli, M.B. Yerer, et al., Natural product-based nanoformulations for cancer therapy: opportunities and challenges, Semin. Canc. Biol. (2019) 1–19.

[12] G. Pandey, N. Deshmukh, V. Science, Usefulness of nanotechnology for herbal medicines, Plant Arch. 13 (2015) 617–621.

[13] H. Amawi, C.R. Ashby, A.K. Tiwari, Cancer chemoprevention through dietary flavonoids: what's limiting? Chin. J. Canc. 36 (2017), 50.

[14] N. Hamzian, M. Hashemi, M. Ghorbani, et al., Preparation, optimization and toxicity evaluation of (SPION-PLGA) ±PEG nanoparticles loaded with gemcitabine as a multifunctional nanoparticle for therapeutic and diagnostic applications, Iran, J. Pharm. Res. 16 (2017) 8–21.

[15] N. Muhamad, T. Plengsuriyakarn, K. Na-Bangchang, Application of active targeting nanoparticle delivery system for chemotherapeutic drugs and traditional/herbal medicines in cancer therapy: a systematic review, Int. J. Nanomed. 13 (2018) 3921–3935.

[16] B.V. Bonifácio, P.B. da Silva, M.A. Ramos, et al., Nanotechnology-based drug delivery systems and herbal medicines: a review, Int. J. Nanomed. 9 (2013) 1–15.

[17] A.K. Sachan, A. Gupta, A review on nanotized herbal drugs, Int. J. Pharma Sci. Res. 6 (2015) 961–970.

[18] Y.H. Choi, H.K. Han, Nanomedicines: current status and future perspectives in aspect of drug delivery and pharmacokinetics, J. Pharm. Investig. 48 (2018) 43–60.

[19] C.L. Ventola, Progress in Nanomedicine: Approved and Investigational Nanodrugs, P.T. 42 (2017) 742–755.

[20] A.K. Gupta, M. Gupta, Synthesis and surface engineering of iron oxide nanoparticles for biomedical applications, Biomaterials 26 (2005) 3995–4021.

[21] Z. Hajikarimi, S. Khoei, S. Khoee, et al., Evaluation of the cytotoxic effects of PLGA coated iron oxide nanoparticles as a carrier of 5- fluorouracil and megavoltage x-ray radiation in DU145 prostate cancer cell line, IEEE Trans. NanoBioscience 13 (2014) 403–408.

[22] K.E. Uhrich, S.M. Cannizzaro, R.S. Langer, et al., Polymeric systems for controlled drug release, Chem. Rev. 99 (1999) 3181–3198.

[23] C. Xu, D. Miranda-Nieves, J.A. Ankrum, et al., Tracking mesenchymal stem cells with iron oxide nanoparticle loaded poly(lactide-co-glycolide) microparticles, Nano Lett. 12 (2012) 4131–4139.

[24] N. Schleich, P. Sibret, P. Danhier, et al., Dual anticancer drug/superparamagnetic iron oxide-loaded PLGA-based nanoparticles for cancer therapy and magnetic resonance imaging, Int. J. Pharm. 447 (2013) 94–101.

[25] F. Matloubi Moghddam, M. Moridi Farimani, S. Taheri, et al., Chemical constituents from Salvia macrosiphon, Chem. Nat. Compd. 44 (2008) 518–519.

[26] S. Khoee, Y. Bagheri, A. Hashemi, Composition controlled synthesis of PCL-PEG Janus nanoparticles: magnetite nanoparticles prepared from one-pot photoclick reaction, Nanoscale 7 (2015) 4134–4148.

[27] S. Khoee, K. Hemati, Synthesis of magnetite/polyamino-ester dendrimer based on PCL/PEG amphiphilic copolymers via convergent approach for targeted diagnosis and therapy, Polymer 54 (2013) 5574–5585.

[28] M. Ashjari, S. Khoee, A.R. Mahdavian, A multiple emulsion method for loading 5-fluorouracil into a magnetite-loaded nanocapsule: a physicochemical investigation, Polym. Int. 61 (2012) 850–859.

[29] M.M. Bradford, A rapid and sensitive method for the quantitation of microgram quantities of protein utilizing the principle of protein-dye binding, Anal. Biochem. 72 (1976) 248–254.

[30] J. Xie, Z. Yang, C. Zhou, et al., Nanotechnology for the delivery of phytochemicals in cancer therapy, Biotechnol. Adv. 34 (2016) 343–353.

[31] X. Bao, M. Gao, H. Xu, et al., A novel oleanolic acid-loaded PLGA-TPGS nanoparticle for liver cancer treatment, Drug Dev. Ind. Pharm. 41 (2015) 1193–1203.

[32] Y. Zhang, X. Chen, C. Gueydan, et al., Plasma membrane changes during programmed cell deaths, Cell Res. 28 (2018) 9–21.

[33] J.R. Eidet, L. Pasovic, R. Maria, et al., Objective assessment of changes in nuclear morphology and cell distribution following induction of apoptosis, Diagn. Pathol. 9 (2014), 92.

[34] Z. Darzynkiewicz, H.D. Halicka, H. Zhao, Analysis of cellular DNA content by flow and laser scanning cytometry, Adv. Exp. Med. Biol. 675 (2010) 137–147.

[35] N. Kekre, C. Griffin, J. McNulty, et al., Pancratistatin causes early activation of caspase-3 and the flipping of phosphatidyl serine followed by rapid apoptosis specifically in human lymphoma cells, Chemother. Pharmacol. 56 (2005) 29–38.

[36] V. Papaliagkas, A. Anogianaki, G. Anogianakis, et al., The proteins and the mechanisms of apoptosis: a mini-review of the fundamentals, Hippokratia 11 (2007) 108–113.

[37] J. Lopez, S.W.G. Tait, Mitochondrial apoptosis: killing cancer using the enemy within, Br. J. Canc. 112 (2015) 957–962.

[38] J.F. Buyel, Plants as sources of natural and recombinant anti-cancer agents, Biotechnol. Adv. 36 (2018) 506–520.

[39] Y. Zhou, A. Zhang, H. Sun, et al., Plant-derived natural products as leads to antitumor drugs, Plant Sci. Today 1 (2014) 46–61.

[40] A.L. Salmela, J. Pouwels, A. Kukkonen-Macchi, et al., The flavonoid eupatorin inactivates the mitotic checkpoint leading to polyploidy and apoptosis, Exp. Cell Res. 318 (2012) 578–592.

[41] A.F.A. Aisha, A.M.S.A. Majid, Z. Ismail, Preparation and characterization of nano liposomes of Orthosiphon stamineus ethanolic extract in soybean phospholipids, BMC Biotechnol. 14 (2014), 23.

[42] D. Bobo, K.J. Robinson, J. Islam, et al., Nanoparticle-based medicines: a review of FDA-approved materials and clinical trials to date, Pharm. Res. 33 (2016) 2373–2387.

[43] R.A. Revia, M. Zhang, Magnetite nanoparticles for cancer diagnosis, treatment, and treatment monitoring: recent advances, Mater. Today 19 (2017) 157–168.

[44] C. Blanco-Andujar, A. Walter, G. Cotin, et al., Design of iron oxide-based nanoparticles for MRI and magnetic hyperthermia, Nanomedicine 11 (2016) 1889–1910.

[45] L. Tong, M. Zhao, S. Zhu, et al., Synthesis and application of superparamagnetic iron oxide nanoparticles in targeted therapy and imaging of cancer, Front. Med. 5 (2011) 379–387.

[46] D.N. Kapoor, A. Bhatia, R. Kaur, et al., PLGA: a unique polymer for drug delivery, Ther. Deliv. 6 (2015) 41–58.

[47] H.B. Nair, B. Sung, V.R. Yadav, et al., Delivery of antiinflammatory nutraceuticals by nanoparticles for the prevention and treatment of cancer, Biochem. Pharmacol. 80 (2010) 1833–1843.

[48] M. Khoobchandani, A. Zambre, K. Katti, et al., Green nanotechnology from brassicaceae: development of broccoli phytochemicals-encapsulated gold nanoparticles and their applications in nanomedicine, Int. J. Green Nanotechnol. 1 (2013), https://doi.org/10.1177/1943089213509474.

[49] A.M. Nassir, N. Shahzad, I.A.A. Ibrahim, et al., Resveratrol-loaded PLGA nanoparticles mediated programmed cell death in prostate cancer cells, Saudi Pharmaceut. J. 26 (2018) 876–885.

[50] A. Mukerjee, J.K. Vishwanatha, Formulation, characterization and evaluation of curcumin-loaded PLGA nanospheres for cancer therapy, Anticancer Res. 29 (2009) 3867–3875.

[51] S. Lecomte, F. Demay, F. Ferri, et al., Phytochemicals targeting estrogen receptors : beneficial rather than adverse effects ? Int. J. Mol. Sci. 18 (2017), 1381.

[52] T. Boam, Anti-androgenic effects of flavonols in prostate cancer, Ecancermedicalscience 9 (2015), 585.

[53] M.K. Sivoňová, P. Kaplán, Z. Tatarková, et al., Androgen receptor and soy isoflavones in prostate cancer, Mol. Clin. Oncol. 10 (2019) 191–204.

[54] S. Estévez, M.T. Marrero, J. Quintana, et al., Eupatorin-induced cell death in human leukemia cells is dependent on caspases and activates the mitogen-activated protein kinase pathway, PloS One 9 (2014), e112536.

[55] N.N. Sarvestani, H. Sepehri, L. Delphi, et al., Eupatorin and salvigenin potentiate doxorubicin-induced apoptosis and cell cycle arrest in HT-29 and SW948 human colon cancer cells, Asian Pac. J. Cancer Prev. 19 (2018) 131–139.

[56] K. Lee, D. Hyun Lee, Y.J. Jung, et al., The natural flavone eupatorin induces cell cycle arrest at the G2/M phase and apoptosis in HeLa cells, Appl. Biol. Chem. 59 (2016) 193–199.

[57] V.P. Androutsopoulos, A.M. Tsatsakis, Benzo[a]pyrene sensitizes MCF7 breast cancer cells to induction of G1 arrest by the natural flavonoid eupatorin-5-methyl ether, via activation of cell signaling proteins and CYP1-mediated metabolism, Toxicol. Lett. 230 (2014) 304–313.

[58] Y. Wang, P. Liu, L. Qiu, et al., Toxicity and therapy of cisplatin-loaded EGF modified mPEG-PLGA-PLL nanoparticles for SKOV3 cancer in mice, Biomaterials 34 (2013) 4068–4077.

[59] C. Huang, Y. Sun, M. Shen, et al., Altered cell cycle arrest by multifunctional drug-loaded enzymatically-triggered nanoparticles, ACS Appl. Mater. Interfaces 8 (2016) 1360–1370.

[60] Y.-C. Lin, J.-Y. Kuo, C.-C. Hsu, et al., Optimizing manufacture of liposomal berberine with evaluation of its antihepatoma effects in a murine xenograft model, Int. J. Pharm. 441 (2013) 381–388.

[61] J. Kim, B.C. Yung, W.J. Kim, et al., Combination of nitric oxide and drug delivery systems: tools for overcoming drug resistance in chemotherapy, J. Contr. Release 263 (2018) 223–230.

[62] S. Korde Choudhari, M. Chaudhary, S. Bagde, et al., Nitric oxide and cancer: a review, World J. Surg. Oncol. 11 (2013), 118.

[63] H. Vahora, M.A. Khan, U. Alalami, et al., The potential role of nitric oxide in halting cancer progression through chemoprevention, J. Cancer Prev. 21 (2016) 1–12.

[64] F. Vanini, K. Kashfi, N. Nath, The dual role of iNOS in cancer, Redox Biol. 6 (2015) 334–343.

[65] H. Koizumi, J. Yu, R. Hashimoto, et al., Involvement of androgen receptor in nitric oxide production induced by icariin in human umbilical vein endothelial cells, FEBS Lett. 584 (2010) 2440–2444.

[66] M. V Cronauer, Y. Ince, R. Engers, et al., Nitric oxide-mediated inhibition of androgen receptor activity : possible implications for prostate cancer progression, Oncogene 26 (2007) 1875–1884.

[67] N.N. Sarvestani, H. Sepehri, M.M. Farimani, Anticancer effect of eupatorin via Bax/Bcl-2 and mitochondrial membrane potential changes through ros mediated pathway in human colon cancer, Int. J. Pharmacogn. Phytochem. Res. 7 (2015) 1039–1046.